

Streamlined construction of a six-channel mouse array coil with 3D printing

Wen-Yang Chiang¹ and Mary P McDougall¹

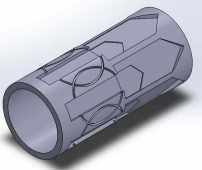
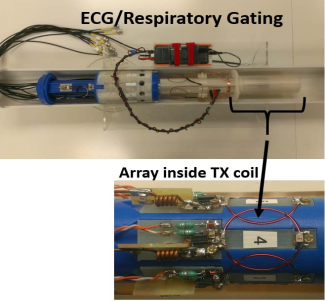
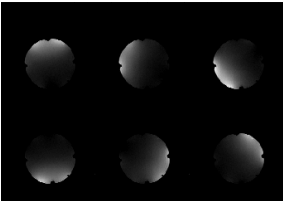
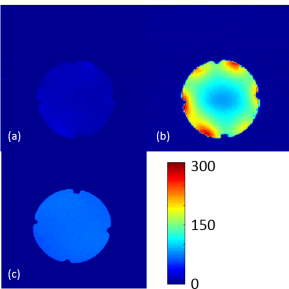
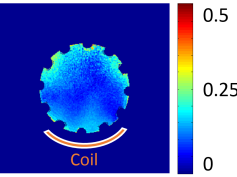
¹Department of Biomedical Engineering, Texas A&M University, College Station, TX, United States

Target Audience: RF engineers involved with small animal coil construction

Purpose: Small animal imaging is inherently challenging due to the associated spatial and temporal resolution demands. The use of array coils is a natural form of relief to consider, particularly as multiple channel receivers are now ubiquitous [1-8]. Fabrication of array coils for small animal imaging is challenging, however, for several reasons mostly associated with miniaturization of the coils and hardware, including but not limited to maintaining sample noise dominance, sensitivity in the element-to-element decoupling process, and lack of space in standard animal scanners and around small formers for traditional hardware such as baluns and cable traps, active decoupling networks, and low input impedance preamplifiers. We report the use of 3D printing for the construction of a six-element mouse array that allowed for **1)** repeatable and optimized geometric decoupling [10], **2)** ease of coil construction with wire elements to maximize coil Q [8,9], and **3)** stable and repeatable field patterns from each element. When compared to a 3.5cm commercial quadrature mouse birdcage, the final constructed array resulted in an average SNR increase of 2.64 times (max = 4.08, min = 1.21), with high-Q, sample-loss dominated, well-decoupled elements with highly consistent field patterns on a compact former design. In addition, 3D printing was used to provide access for and manage the ECG and respiratory gating wires and to fabricate a nose cone for isoflurane delivery that was customized for the coil fixture.

Methods: **1) Optimized and repeatable geometric decoupling:** The diameter of each loop coil was determined by the percentage of overlap used for geometric decoupling: Diameter of loop coil = (circumference of coil former) / 6 / (1 - percentage of overlap). To demonstrate the precision/utility of 3D printing for the application, four coil formers with 23%, 25%, 27% and 28% of overlap were printed using an in-house assembled Replicator 2 3D printer (MakerBot, NY) using PLA material. Because no glue was needed – just a pressure fit in the printed former – coil components were easily exchangeable. For each coil former, two adjacent coils with AWG 22 wire and tune/match boards were fitted inside of the etched pattern. When the best-case overlap was determined using standard S_{21} measurements, the former (ID = 31.75 mm and OD = 38.1 mm) with six etched wire loop coils and tune/match boards was designed in SolidWorks software as shown in Fig. 1. **2) High-Q wire elements:** The former was populated straightforwardly with pressure-fit only construction for the wire coils and match/tune boards, as shown in Fig. 2. Loaded and unloaded Q measurements were acquired to demonstrate coil quality and sample loss dominance. **3) Repeatability and consistency of field patterns:** Imaging of a 3D printed cylindrical phantom (ID = 27.5 mm, inner length = 57 mm) filled with 1 g/L CuSO₄ and 5.4 g/L NaCl was performed on a 4.7T/40cm Varian Inova scanner with TE = 30 ms, TR = 1000 ms, FOV = 50 mm x 50 mm, matrix size = 256 x 128, slice thickness = 1 mm. The SNR achieved by the six-channel array was compared to 1) the transmit coil – a linear birdcage coil built in-house (ID = 55 mm, OD = 84 mm) with four active detune traps and 2) a commercial Varian 3.5cm diameter quadrature birdcage. Inter-element consistency was shown by rotating the individual field patterns of each element into alignment with one another and calculating/mapping the standard deviation between the elements (normalized to the mean intensity of the six elements) on a pixel-by-pixel basis.

Results and discussion: The best-case geometric decoupling out of the tested cases was S_{21} = -17.4 dB at 27% overlap, when the diameter of the loop coil was 27.32 mm. As an example of the fine-tuning enabled by the 3D printing, when the overlap was 28%, the geometric decoupling between adjacent channels was -9.3dB even though the change in diameter was only 400 μ m. The unloaded to loaded Q ratio was 142.8/101.7 = 1.4, indicating high quality coils and sample loss dominance. The phantom images received by the individual loop coils indicated clearly isolated and consistent field patterns, as shown in Fig 3. In addition, as seen in Fig. 4a, the homogeneity of the transmit coil image verified the absence of coupling between the transmit coil and the receive array. Figures 4b-c indicates the sum-of-squares reconstruction showed an average SNR increase over the Varian quad birdcage of 2.64 times (max = 4.08, min = 1.21), slightly inflated by the sum-of-squares reconstruction from single-channel imaging (versus parallel reception with correlated noise). The mapping of the normalized standard deviation between the field patterns of the six elements is shown in Fig. 5, indicating highly consistent/repeatable patterns from each element (mean S.D. = 0.15, max = 0.23, min = 0.07). In summary, the use of 3D printing enabled the ease of fabrication of stable, high-performing coil elements for a six-channel mouse array. Our immediate future work is to use the 6-channel mouse array to perform *in vivo* mouse parallel imaging with ECG and respiratory gating.

				
<p>Fig 1. SolidWorks rendering of former with etched pattern of coils and tune/match boards</p>	<p>Fig 2. Top: entire array assembly, including Tx coil (covering the array) and the ECG/respiratory gating wires entering from the middle of the former. Bottom: uncovered and zoomed array.</p>	<p>Fig 3. Phantom images received from individual loop coils indicating good isolation and repeatability.</p>	<p>Fig 4. SNR maps from: (a) linear transmit coil, (b) 6-ch mouse array, and (c) Varian mouse quadrature birdcage coil.</p>	<p>Fig 5. Mapping of the normalized standard deviation between the field patterns of the six elements.</p>

References: [1] J.E. Schneider et al. *Mag. Res. Med.*, vol. 59, pp. 636-641, 2008. [2] D. Gareis et al. *NMR in Biomed.*, vol. 20, pp. 326-334, 2007. [3] M.S. Ramirez et al. *Mag. Res. Med.*, vol. 63, pp. 803-810, 2010. [4] O. Dietrich et al. *Proc. ISMRM*, 2007, pp. 1759. [5] J.X. Wang et al. *Proc. ISMRM*, 2010, pp. 1489. [6] T. Lanz et al. *Mag. Res. Med.*, vol. 64, pp. 80-87, 2010. [7] M. Tabbert et al. *Proc. ISMRM*, 2010, pp. 4735. [8] B. Keil et al. *Mag. Res. Med.*, vol. 66, pp. 582-593, 2011. [9] G. Wiggins et al. *Mag. Res. Med.*, vol. 62(3), pp. 754-762, 2009. [10] P.B. Roemer et al. *Mag. Res. Med.*, vol. 16 pp. 192-225, 1990.